

IMMI's performance with different seismic acquisition parameters and random noise

Sergio Romahn and Kris Innanen

ABSTRACT

IMMI stands for iterative modelling, migration and inversion. It proposes to incorporate standard processing techniques into the process of full waveform inversion (FWI). Following IMMI's philosophy, we use a phase shift plus interpolation (PSPI) migration with a deconvolution imaging condition to obtain the gradient, and well velocity to scale the gradient into a velocity perturbation. The above contrasts with the use of a two-way wave migration method (such as reverse time migration RTM), and the use of an approximation of the inverse Hessian matrix or a line search to find the scale, as is done in standard FWI. We show the suitability of estimating the subsurface velocity model by applying IMMI's approach using a synthetic example. The results confirm that the gradient obtained with PSPI provides an adequate direction to minimize the objective function, and that well calibration produces an efficient scale to convert the gradient into a velocity perturbation. We evaluated the performance of the inversion when the maximum offset and the source interval are changed with and without the presence of random noise. Generally speaking, larger offsets and higher shot density generate better results, specially in the presence of noise. Higher folds, produced by large offsets and small source interval, improve the inversion result because the gradient is obtained by stacking the migrated data residuals.

INTRODUCTION

The objective of full waveform inversion is to estimate properties of the subsurface based on the solution of the inverse problem for seismic data (Tarantola, 1984). Margrave et al. (2010) described the process as an iterative cycle that involves four main steps:

The four steps of the FWI's cycle are:

- 1) Generating synthetic seismic data (predicted data $\Psi_{r,k}$) from a very smoothed initial model v_o , and calculating the data residual $\delta\Psi_{r,k} = \Psi_r - \Psi_{r,k}$.
- 2) Pre-stack depth migration using the current velocity model ($v_{k-1} = v_o$, for iteration 1) of the data residual and stack $M(\delta\Psi_{r,k})$. This provides the gradient or update direction.
- 3) Scaling or "calibrating" the gradient that produces the velocity perturbation δv_k .
- 4) Updating the current velocity model $v_k = v_{k-1} + \delta v_k$, which will be used in the next iteration.

Lailly (1983) and Tarantola (1984) showed that the depth migration of the data residual produces the gradient of the objective function, which is defined in Equation 1.

$$\phi_k(x, z, w) = \sum_{s,r} (\Psi - \Psi_k)^2 \quad (1)$$

The gradient is the element in the minimization scheme that provides the direction of the velocity update. The other element modifies the length of the gradient and can be found as the inverse Hessian or an approximation. If the inverse Hessian is replaced by a scalar λ , the mathematical effort is reduced to the gradient or steepest-descent method.

Equation 2 represents the velocity model update in terms of the scalar λ and the gradient of the objective function. The gradient is the result of crosscorrelating the incident wave field emitted from the source $\hat{\Psi}_s(x, z, \omega)$ with the back-propagated residual wavefield $\hat{\Psi}_{r(s),k}^*(x, z, \omega)$ over a frequency range. This is a two-way wave migration. The scale λ is commonly estimated by a line-search method which requires an extra forward problem per shot (Virieux and Operto, 2009).

$$\delta v(x, z) = \lambda \nabla_v \phi_k(x, z, w) = \lambda \int \sum_{s,r} \omega^2 \hat{\Psi}_s(x, z, \omega) \delta \hat{\Psi}_{r(s),k}^*(x, z, \omega) d\omega \quad (2)$$

IMMI was introduced by Margrave et al. (2012), it was thought as an alternative to accomplish FWI by using tools already available and widely used in seismic processing. Examples of the IMMI's philosophy are the application of any depth migration method and the incorporation of well information for scaling the gradient. Furthermore; the authors argue that using a deconvolution imaging condition, instead of the correlation used in RTM, achieve something very similar to the application of the main diagonal elements of the inverse Hessian, that can be seen as a gain correction, as was shown by Shin et al. (2001). Pan et al. (2014) applied IMMI and compared the crosscorrelation and deconvolution imaging conditions. The showed that using a deconvolution based gradient compensates the geometrical spreading.

Following IMMI's approach, we use the phase shift plus interpolation (PSPI) migration method (one-way wave migration) with a deconvolution imaging condition to obtain the gradient. PSPI, introduced by Gazdag and Sguazzero (1984), allows using a range of frequencies of interest which is very convenient to explore frequency employment strategies in FWI. Pratt (1999) suggested that starting the inversion using low frequencies and then move to higher ones may help to avoid local minima. We followed this strategy.

We estimated the scale λ in the form of a match filter by using well velocity information. We will show this process in the following section

We will present the process of FWI within the perspective of IMMI with a synthetic example. Then we will modify the maximum offset and the source interval in order to see how the inversion result is affected. Finally, we will add random noise and compare the results.

IMMI'S PROCESS

True velocity model and observed shots

The true velocity model corresponds to a shallow synclinal that constitutes a reservoir trap. The reservoir is characterized by a low P-wave velocity surrounded by a high velocity medium (figure 1). Synthetics shots were generated by solving the acoustic wave equation by finite differences. The wavelet is minimum phase with a dominant frequency of 20 Hz. These shots will be considered the observed ones. The acquisition parameters for this case are: source interval = 100 m, receiver interval = 10 m, maximum offset = 2000 m, fold = 20, number of shots = 81. The first, middle and last shots are shown in figure 2.

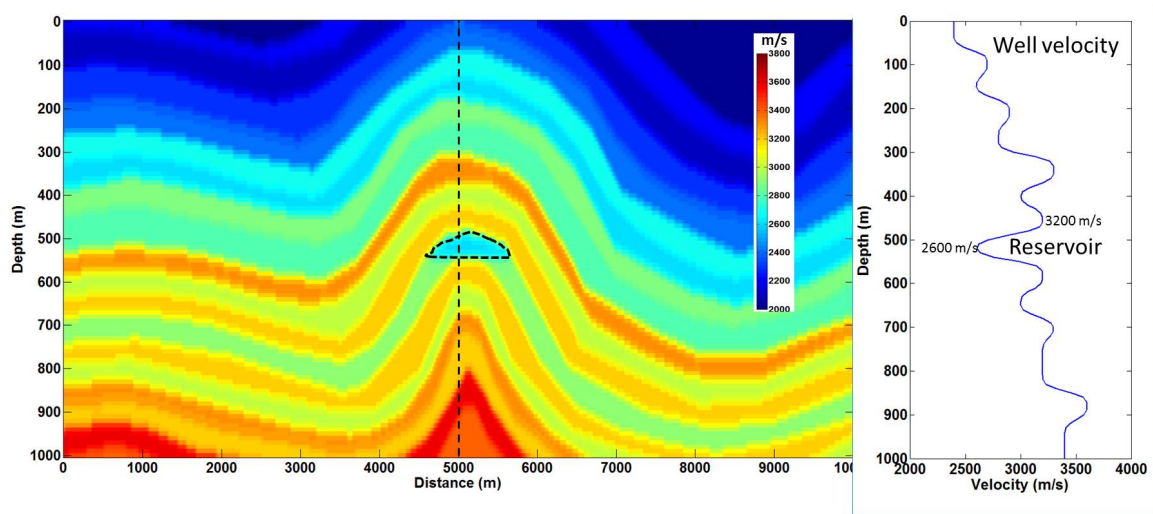


FIG. 1. True velocity model

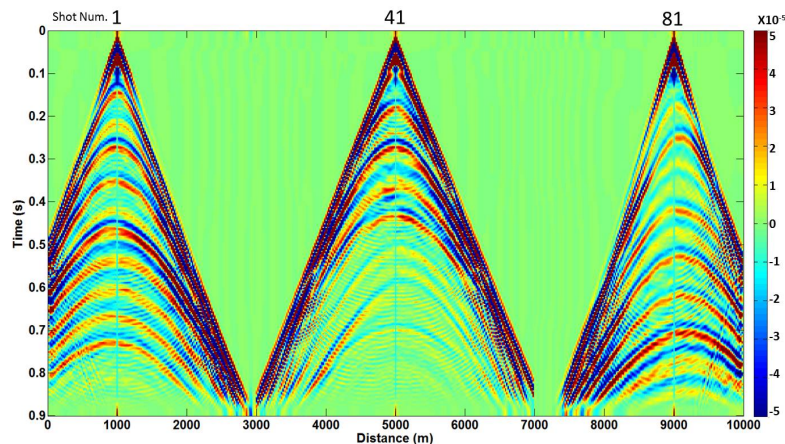


FIG. 2. Observed shots.

The design of the seismic survey contemplated fold taper and migration apron to define a zone where the performance of the inversion will be evaluated. The error in the model will be measured in the zone of migration with full fold and no border effects (figure 3).

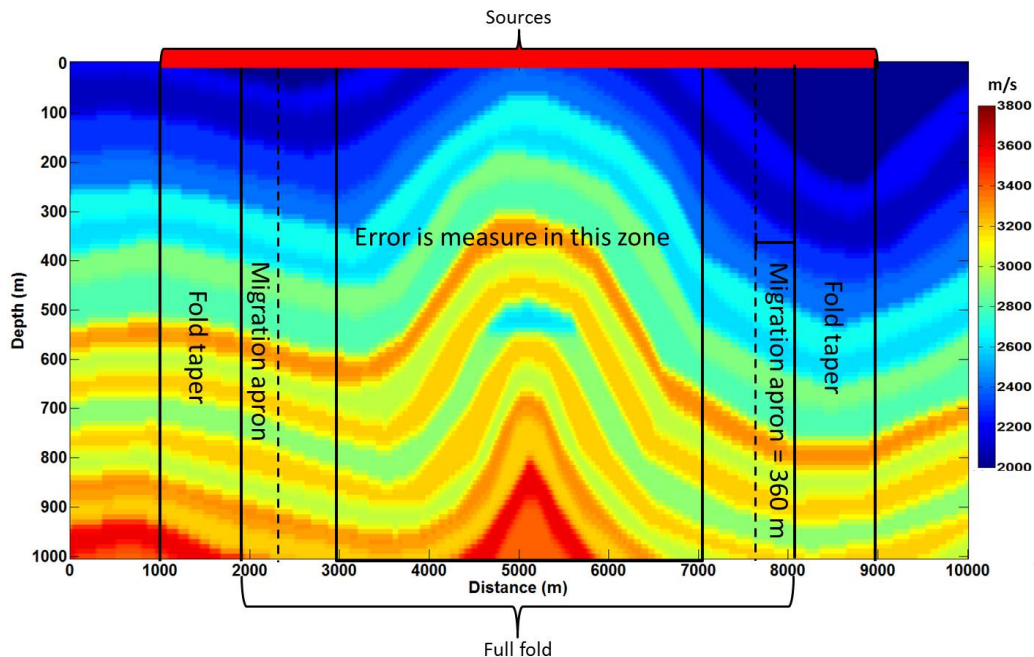


FIG. 3. The inversion performance will be evaluated in the zone with full seismic coverage.

First iteration

The first iteration was done with an initial velocity model that was constructed by applying a Gaussian smoother to the true velocity model with a half-width of 290 m (figure 4). We compared the reflectivity amplitude spectra of the initial and true model to the seismic amplitude spectrum in the location of well B. The initial model provides low frequencies between zero and 2 Hz. The seismic data contain information above 5 Hz. There is a gap between 3 and 4 Hz where neither the initial model nor the seismic data contribute. The true velocity model and the seismic have a frequency pick around 12 Hz, which is related to the average period of 0.08 seconds in the model. Well C was used in the process of gradient calibration.

An observed shot, a shot modelled with the initial model, and the data residual, are displayed in figure 5. The direct arrival is virtually the only event in the modelled shot because the smoothed initial model does not contain any significant velocity contrasts. Therefore, the data residual is mainly the observed shot with an attenuated direct arrival. Figure 6 shows the depth migration of data residual by using a PSPI method. We applied a mute and stacked all the migrated differences to build the gradient. Note that the order of magnitude of the gradient is minus 5. We are using a frequency range from 1 to 6 Hz for the first iteration.

The next step is to scale the gradient. Well calibration reduces the computational cost because we don't need an extra forward modeling as it is done in the line search method. The calibration process was described by Margrave et al. (2010). Firstly, the difference between the well and the initial model velocities δvel is calculated. Then, an amplitude

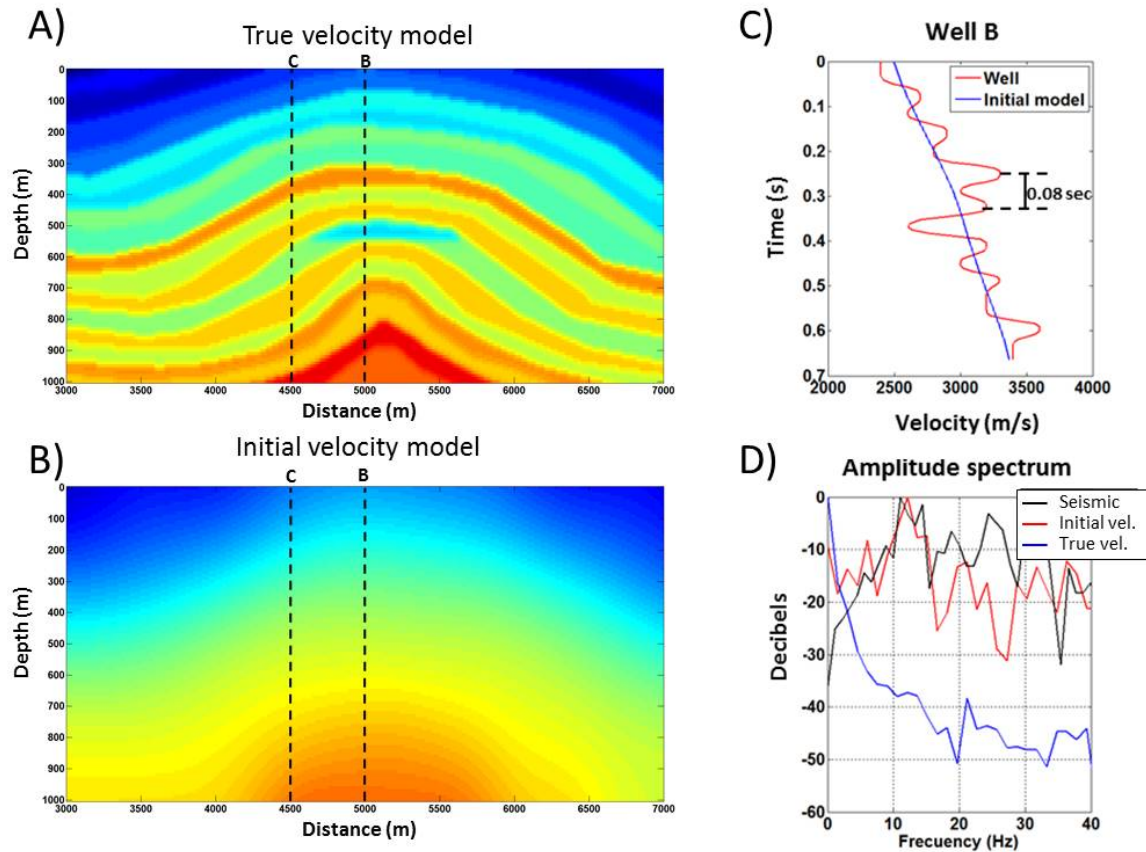


FIG. 4. A) True velocity model. B) Initial velocity model. C) Initial and true velocity curves in well B. D) Amplitude spectra of seismic, true and initial velocity models.

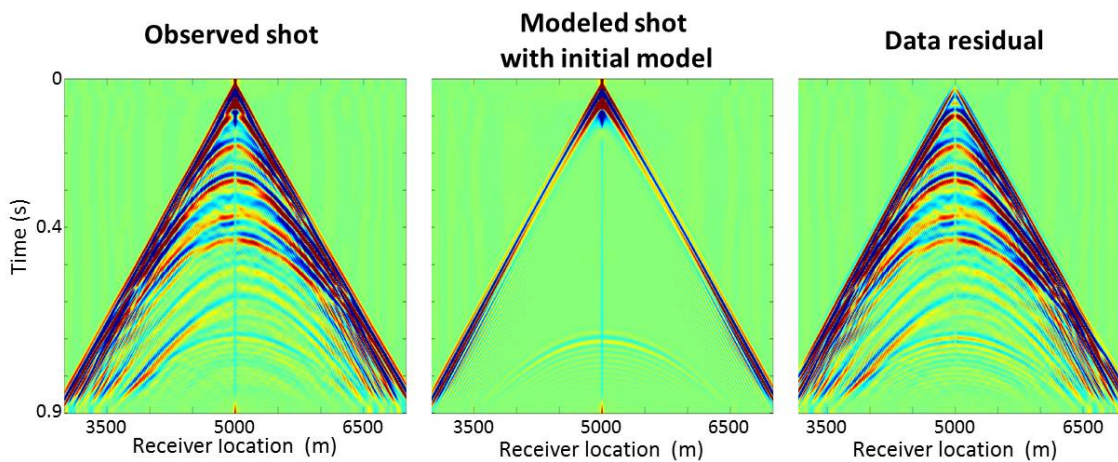


FIG. 5. The data residual is the difference between observed and modeled shots.

scalar a and phase rotation ϕ , that make the gradient trace g in the well location more like δvel , are estimated. The scalar a is found such that $\delta vel - ag$ is minimized by least squares. Finally, a convolutional match filter is estimated with a and ϕ , which is applied to all the

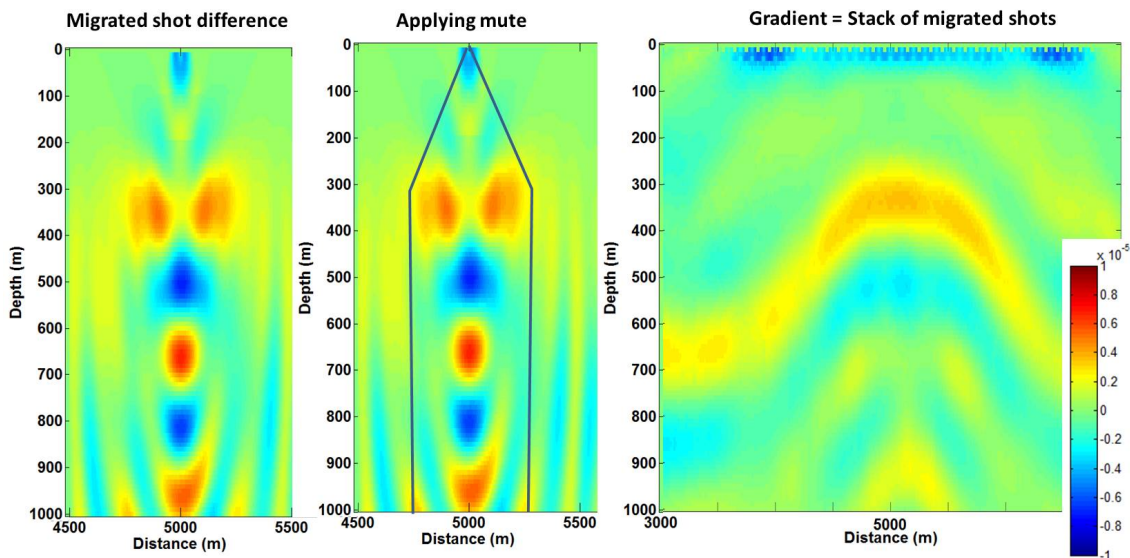


FIG. 6. Depth migration of the data residual. The gradient is the result of stacking all the migrated data residuals. A mute before stacking is helps to avoid artifacts in the gradient.

gradient traces to obtain the velocity update. The gradient after scaling has a magnitude order of 2. Figure 7 shows this process.

The final step of the cycle is to add the velocity update to the current velocity model (figure 8). These new model is the one that will be used in the next iteration.

More iterations

The frequency band regularly increased 1 Hz in each iteration, as shown in Table 1. We measured the error in the blind and calibration wells, and the error in the model. These indicators will be analyzed to evaluate the performance of the inversion.

Table 1. Frequency range used in each iteration.

Iteration	Frequency band (Hz)
1	1-6
2	2-7
3	3-8
⋮	⋮
15	15-20

Figure 9 shows the behavior of the inverted velocity in the blind and calibration well, as well as the error for both cases. The error was calculated as $max(sum(abs(V_w - V_i)))$, where V_w is the well velocity and V_i is the inverted velocity. The normalized error was obtained by taking the error for the first iteration as reference. The inverted velocity highly resembles the true velocity in the calibration well location. Its error sharply decreases in the first iteration, it is very similar for iterations 2 and 3; then, it is steadily reduced from iteration 4 to 9, when we cover frequencies from 5 to 15 Hz. When the maximum frequency

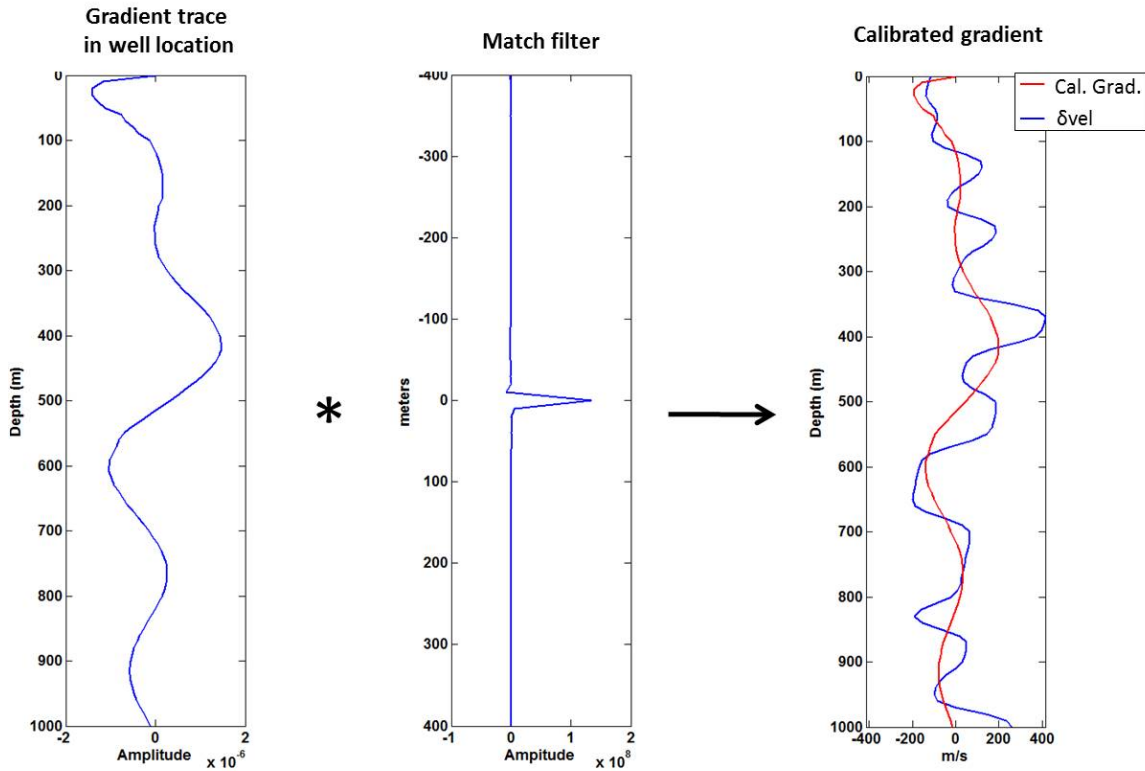


FIG. 7. The gradient trace is scaled to be like the difference between the well and the initial model velocities at the well location.

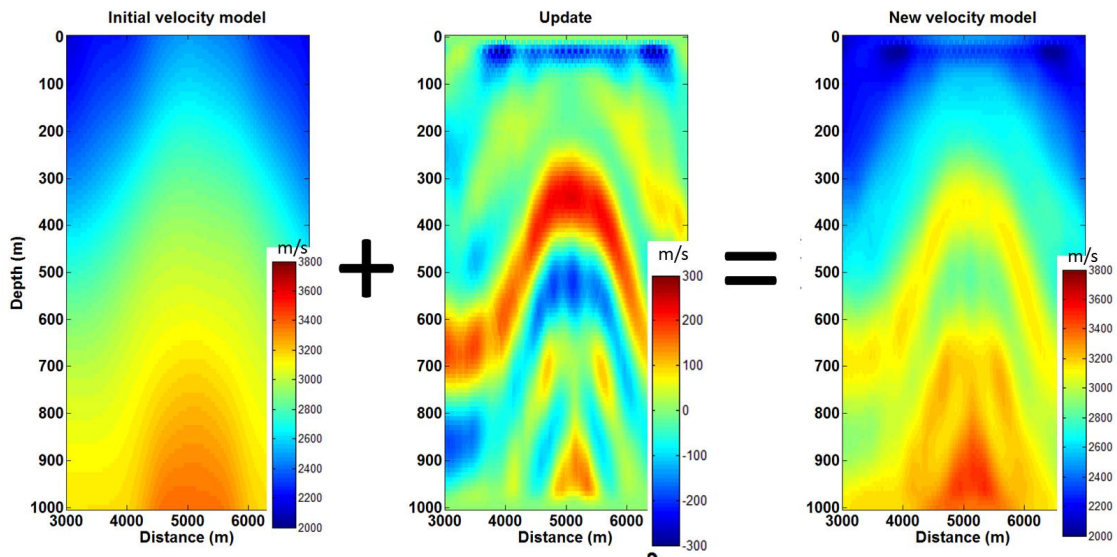


FIG. 8. The sum of initial velocity model and the velocity update results in a new velocity model that will be used in the next iteration. Note the color bar of the update is from -300 to 300 m/s.

is greater than 15 Hz, the inversion does not longer improve. The error in the blind well has a similar behavior than in the calibration well, it reaches its minimum in iteration 9. When

we go to higher frequencies it starts to increase. The inverted velocity curve develops a pick below 500 m after iteration 13. In general, the inversion tends to be better in the vicinity of the calibration well. It is remarkable that the error always decreases in the calibration well, even if we go to higher frequencies.

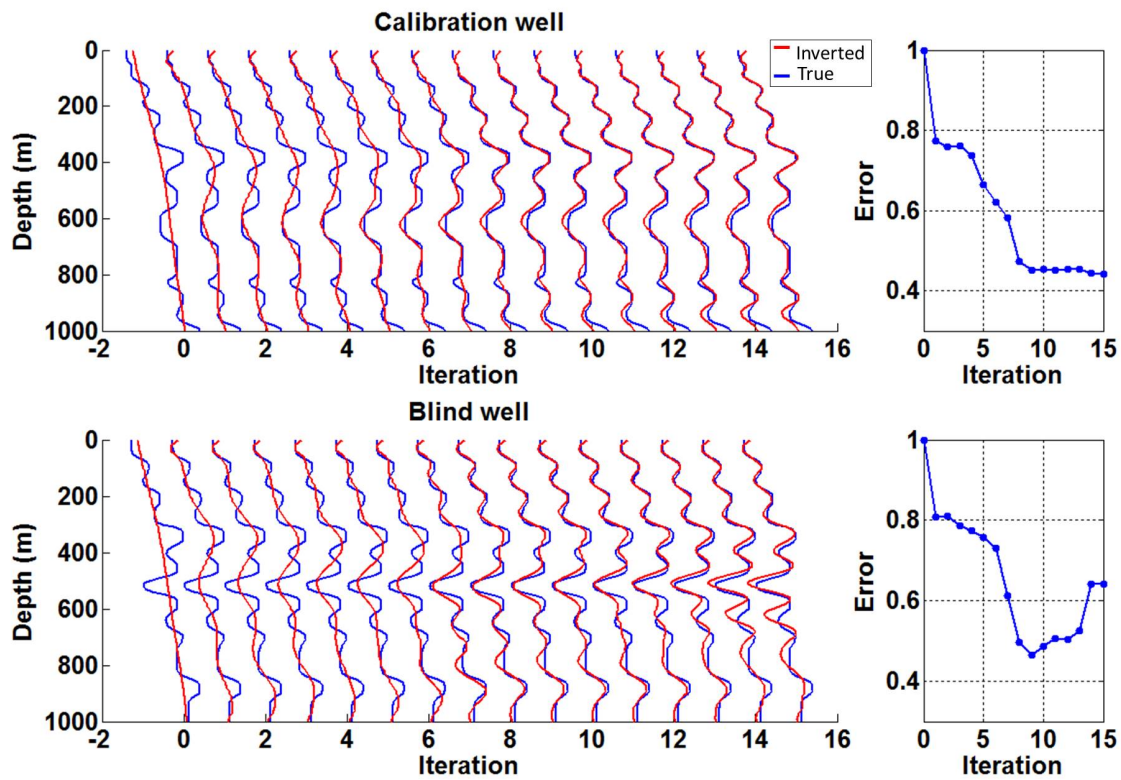


FIG. 9. Inversion performance in the calibration and blind well locations.

The error in the shots was calculated as the L2-norm of the difference between the observed and the modelled shots. Figure 10 shows an observed and a modelled shots and its difference for iteration 15. The modelled shot mimics the main seismic events of the observed shot; however, the data residual shows details that couldn't be reconstructed by the inverted model. The L2-norm of the data residual steadily decreases in each iteration.

Figure 11 shows the comparison among the initial, final-inverted and true velocity models. With this synthetic example, we showed that IMMI is able to obtain the subsurface velocity from the seismic shots by using a one-way wave migration method and well calibration. The 500-m depth reservoir has been well discriminated from the rocks that surround it.

The location of the calibration and blind well are displayed in the models and their error curves are compared to the error in the whole model. The error curves are very similar, being slightly better the inversion at the calibration well location.

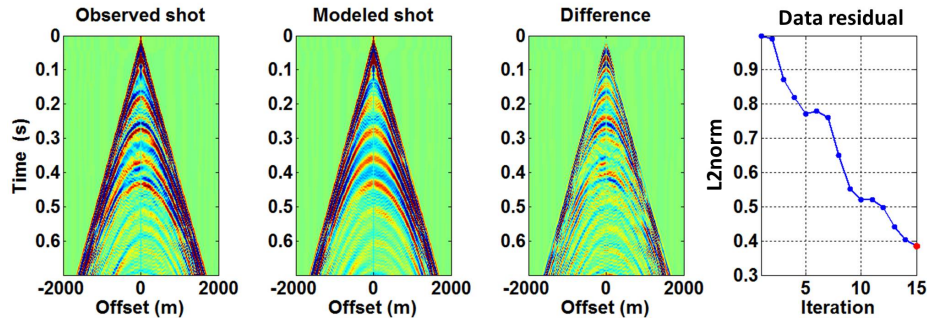


FIG. 10. The shot error is calculated applying the L2 norm to the difference between the observed and modeled shots.

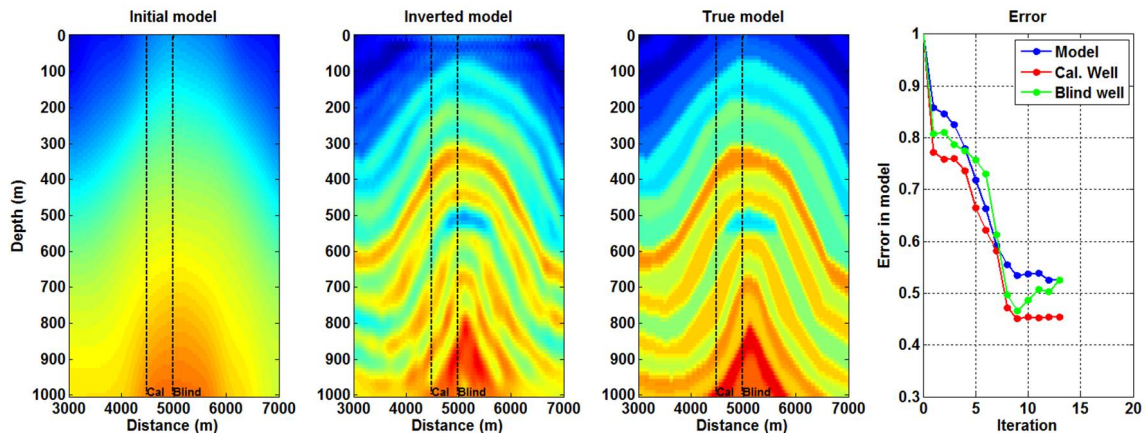


FIG. 11. Initial, inverted and true velocity models at iteration 13. The error curves are very similar, being slightly better the inversion at the calibration well location.

INVERSION PERFORMANCE WHEN VARYING MAXIMUM OFFSET AND SOURCE INTERVAL WITH AND WITHOUT RANDOM NOISE

We will compare the performance of the inversion with different acquisition parameters and when random noise is present. We will vary the maximum offset in the first test. When we change this parameter, we also vary the total fold as shown in Table 2. We add some random noise and vary the maximum offset in the second experiment. The third experiment consists in varying the source interval, which also modifies the total fold and the number of shots (Table 3). We add random noise and vary the source interval in the last test.

Table 2. Varying maximum offset

RI (m)	SI (m)	Max offset (m)	Fold	Channels	Number of shots
10	100	500	5	101	81
10	100	1000	10	201	81
10	100	1500	15	301	81
10	100	2000	20	401	81

Table 3. Varying source interval

RI (m)	SI (m)	Max offset (m)	Fold	Channels	Number of shots
10	20	2000	100	401	401
10	50	2000	40	401	161
10	100	2000	20	401	81
10	250	2000	8	401	33

Inversion performance when varying maximum offset

The maximum offset is a critical parameter in the acquisition of seismic data. The rule of thumb says that we need at least offsets as large as the deeper target (Cordsen et al., 2000). We compare the inversion result with four different maximum offsets: 500, 1000, 1500 and 2000 m. The reservoir is located at a depth of 500 m; however, we want to obtain an inverted velocity model up to 1000 m. A qualitative comparison of the inversion is shown in figure 12. The results correspond to the 13th iteration and the four maximum-offset scenarios. The observed shot, modelled shot and the data residual are plotted at the left side. The inverted and true velocities for the blind and calibration well are shown in the middle. The inverted velocity model is displayed in the right side. The maximum time is 0.9 seconds, which is enough to record the maximum offset of 2000 m. Offsets larger than 2000 m do not contribute to the maximum depth model of 1000 m. The reservoir is located at a time of 0.37 seconds, and the deeper reflector time is at 0.6 seconds. If we observe the blind and calibration wells, we see that the four cases are able to resolve the reservoir; however, the shallow part is better inverted when we use offsets of 1000 m or larger. Events deeper than the reservoir are better inverted with offsets of 1500 m or larger. The velocity in the reservoir is slightly overestimated when we use offsets of 1500 or 2000 m.

A quantitative assessment is shown in figure 13. The L2-norm of the data residual behaves very similar in the four scenarios. It dramatically decreases after the 7th iteration when we use frequencies above 12 Hz. When we reach the frequency of 15 Hz (10th iteration), it continues decreasing in a smaller rate. The maximum offset of 2000 m provides the smallest error as we add more iterations. The error in the blind well shows that the inversion is poor when we use offsets of 500 m. As we increase the maximum offset, the error tends to be smaller. We note that the error starts to increase around the iteration 10, which does not occur in the calibration well. In general, the inversion is better in the calibration well. This means that the gradient is been optimally scaled in the well location where produces the best result.

This experiment has shown that offsets, even twice as larger than the target depth, favorably contribute to the inversion.

Inversion performance when varying maximum offset in the presence of noise

When we increase the maximum offset, we also augment the total fold, which contributes to improve the signal to noise ratio. We want to know the effect of increasing the maximum offset in the presence of random noise. The level of noise used in this exercise

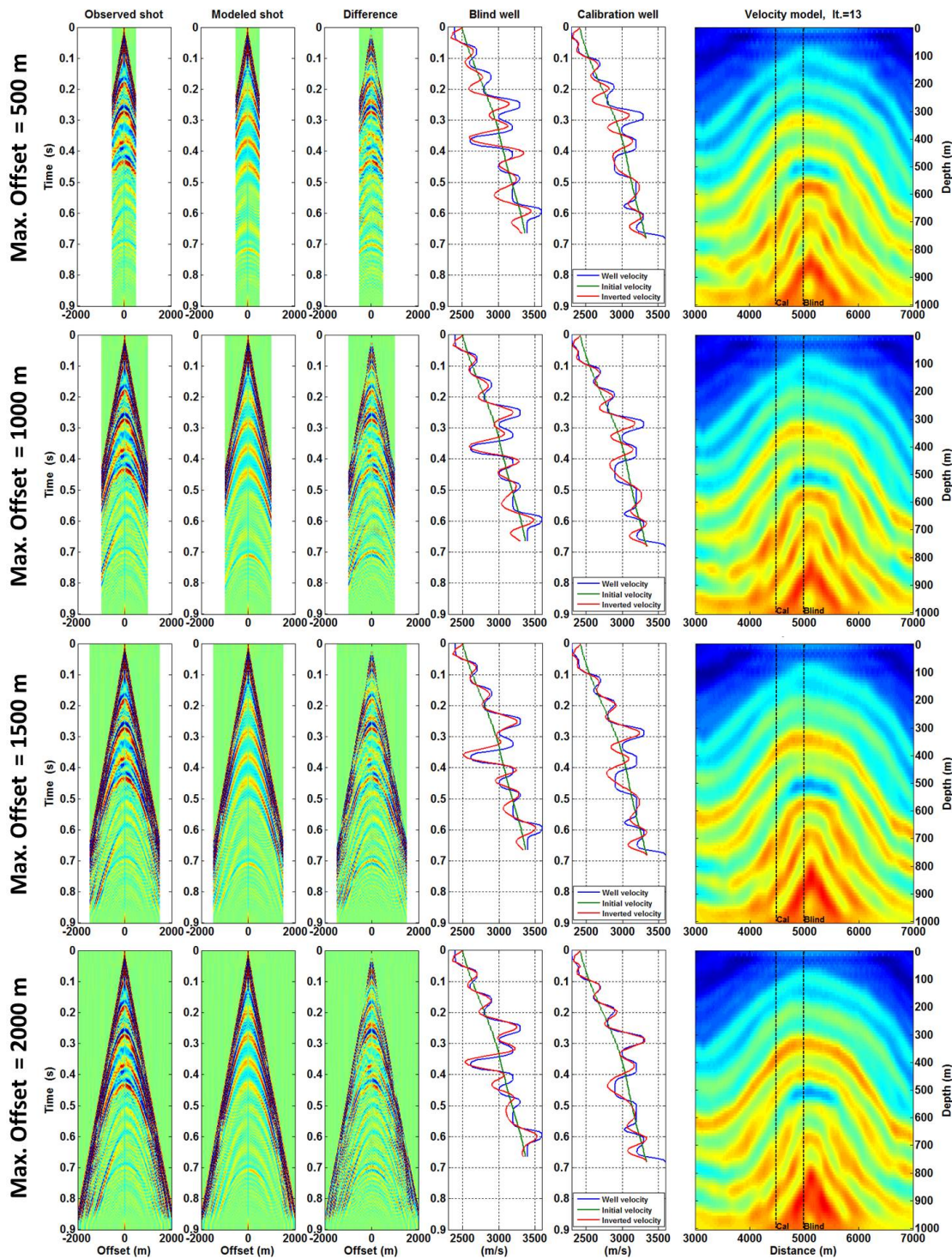


FIG. 12. Maximum offset of 500, 1000, 1500 and 2000 m were used to evaluate the inversion's performance. The inversion outcome is shown for the 13th iteration.

corresponds to a signal to noise ratio (S/N) of 6.

The comparison of the inverted velocity models with and without noise for the 2000-m

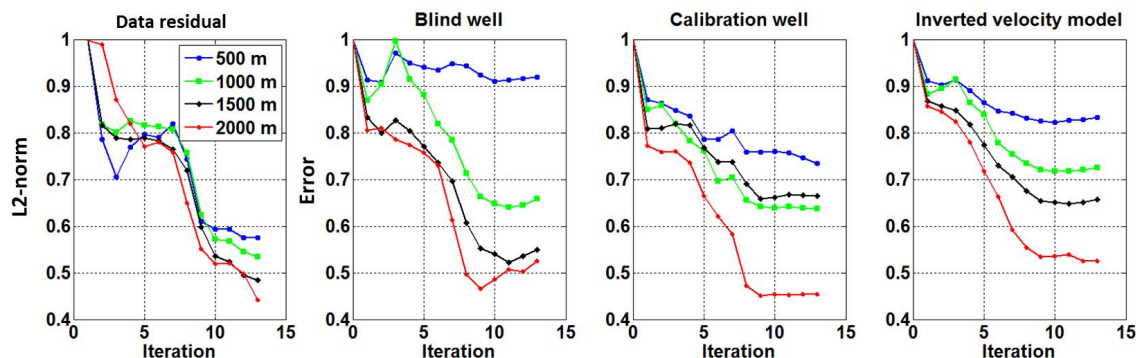


FIG. 13. Normalized error when varying maximum offset with no noise.

offset case is shown in figure 14. The damaging effect of random noise in the inversion is evident.

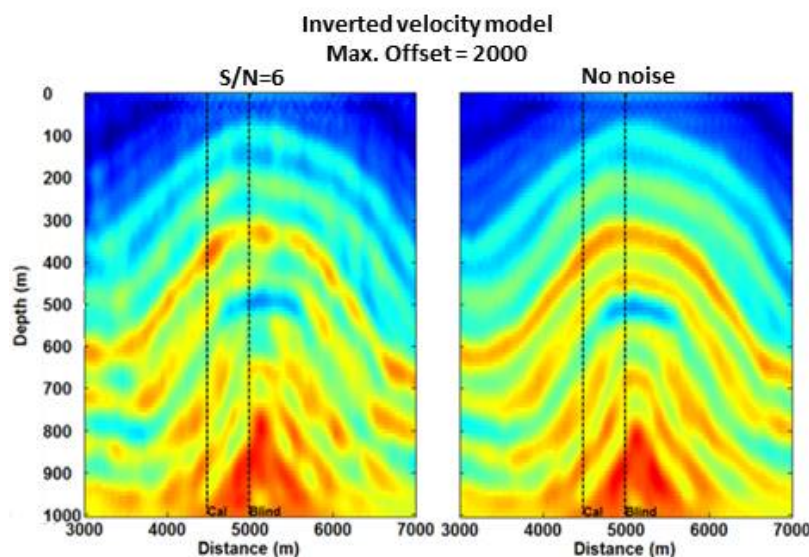


FIG. 14. Inverted velocity model with and without noise using a maximum offset of 2000 m.

We contrasted the error for the four maximum-offset scenarios with and without noise in figure 15. Larger offsets provide better results, as we expected. We found interesting differences when comparing small vs large offsets. The error curves are very similar with and without noise for the 500-m offset case, meaning that any inversion with small-offset traces may not be improved, even if we rise the S/N with processing techniques. On the other hand, when we have large offsets, there is still room to obtain better results if we increase the S/N by applying attenuation noise techniques in the shot domain. It is interesting that the error always decreases even with noise for a 2000-m offset in the calibration well.

Inversion performance when varying source interval

We used three different source intervals (SI) for this experiment: 250, 100 and 50 m. The total fold varies as 8, 20 and 40, respectively. The maximum offset was kept at 2000 m

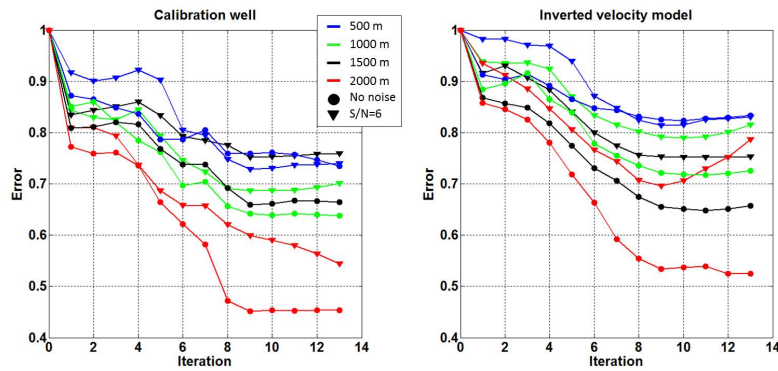


FIG. 15. Normalized error when varying maximum offset with and without noise.

and no noise was added. Figure 16 shows how the inverted velocity model is affected with different SI. We observe a strong foot print when the source interval is 250 m, the inversion cannot recover the detail of the anticline's top below the reservoir, and the layers above appear discontinuous. All these issues are mitigated when the source interval is equal to 100 m. A SI=50 m produces a similar result as a SI=100 m. The plots of the errors (figure 17) confirm the qualitative assessment. The error is consistently higher for a SI=250 m, while the error curves for 100 and 50 m are practically the same. The fact that we are not considering noise, does not allow seeing the advantage of increasing the number of shots and the fold. This case will be shown in the next experiment.

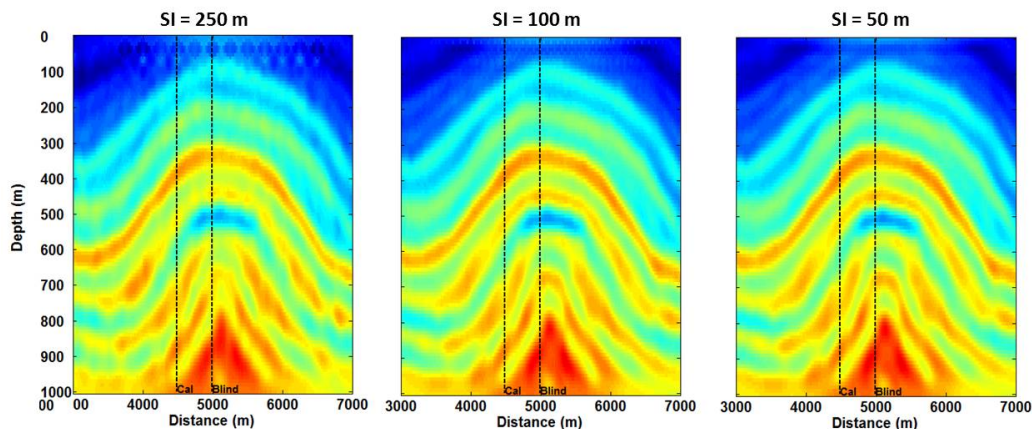


FIG. 16. Effect of varying the source interval in the inversion result. No noise was added. The inverted velocity models for SI = 50 m and SI = 100 m are practically the same.

Inversion performance when varying source interval in the presence of noise

The fact that the gradient is obtained by stacking the migrated data residuals, suggests that as the fold increases, the S/N should also increase, which may result in better inverted models. We evaluate this hypothesis in this experiment.

Figure 18 shows the inverted velocity models for four different source intervals: 250, 100, 50 and 20 m. The corresponding folds are 8, 20, 40 and 100. We are keeping the

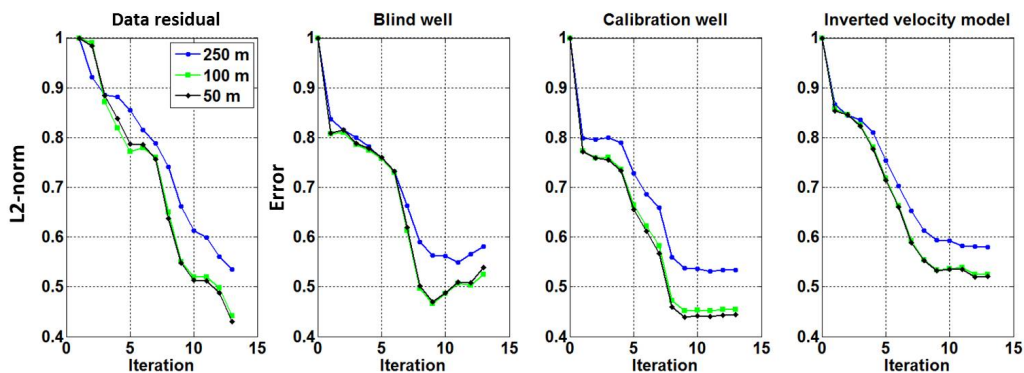


FIG. 17. Error when varying the source interval with no noise.

maximum offset constant in 2000 m. Random noise related to a $S/N=6$ was added. Qualitatively, we can identify the reservoir in the four cases; however, it is better defined with a source interval smaller than 100 m. The layers are more continuous and the top of the anticline is better defined with source intervals of 50 and 20 m. The benefit of decreasing the source interval can be better seen in the error plots (figure 19). The tendency is that the inversion is enhanced as the number of shots increases.

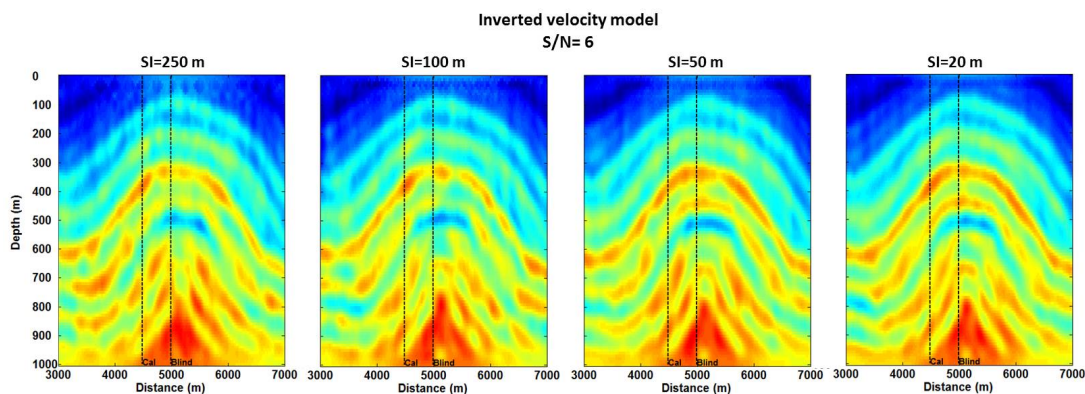


FIG. 18. Inverted velocity model with and without noise using different source intervals.

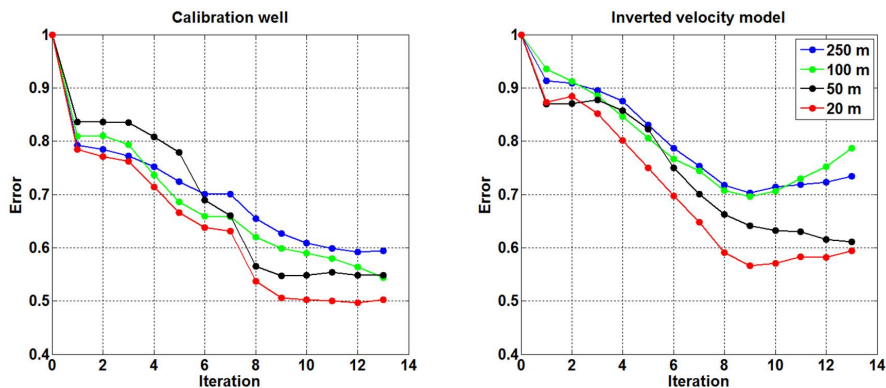


FIG. 19. Normalized error when varying source interval with and without noise.

CONCLUSION

We showed that IMMI's approach for FWI is able to find the P-wave velocity model of the subsurface in an acoustic context and with synthetic data. Within IMMI's philosophy, we proved that other depth migration techniques, such as PSPI, are suitable for obtaining the gradient in the minimization scheme of FWI. We also showed that well calibration provides an optimal scaling of the gradient in the vicinity of the well, and it still acceptably works as we go away from the well location.

The result of the inversion is strongly influenced by random noise and acquisition parameters of the seismic survey. If we consider the rule of thumb of maximum offset equals deeper target, the inversion of the model may be compromised. We observed that offsets as large as twice the maximum target depth, favorably contribute to the inversion.

The gradient is obtained by stacking the migrated data residuals. The increment of fold, produced by smaller shot intervals and larger offsets, plays an important role for the improvement of the inversion. Generally speaking, larger offsets and higher shot density increase the fold, which improves the performance of the inversion in the presence of noise.

ACKNOWLEDGEMENTS

We thank the sponsors of CREWES for their support. We also acknowledge support from NSERC through the grant CRDPJ 461179-13. Author 1 thanks PEMEX and the government of Mexico for founding his research.

REFERENCES

- Cordsen, A., Galbraith, M., Peirce, J., and Hardage, B. A., 2000, Planning land 3-D seismic surveys, vol. 9: Society of exploration geophysicists Tulsa.
- Gazdag, J., and Sguazzero, P., 1984, Migration of seismic data by phase shift plus interpolation: *Geophysics*, **49**, No. 2, 124–131.
- Lailly, P., 1983, The seismic inverse problem as a sequence of before stack migration: *SIAM*, 206–220.
- Margrave, G. F., Ferguson, R. J., and Hogan, C. M., 2010, Full-waveform inversion with wave equation migration and well control: CREWES Research Report, **22**.
- Margrave, G. F., Innanen, K. A., and Yedlin, M., 2012, A perspective on full-waveform inversion: CREWES Research Report, **24**.
- Pan, W., Margrave, G. F., and Innanen, K. A., 2014, Iterative modeling migration and inversion (immi): Combining full waveform inversion with standard inversion methodology: 84th Ann. Internat. Mtg., SEG, Expanded Abstracts, 938–943.
- Pratt, R. G., 1999, Seismic waveform inversion in the frequency domain, part 1: Theory and verification in a physical scale model: *Geophysics*, **64**, No. 3, 888–901.
- Shin, C., Yoon, K., Marfurt, K. J., Park, K., Yang, D., Lim, H. Y., Chung, S., and Shin, S., 2001, Efficient calculation of a partial-derivative wavefield using reciprocity for seismic imaging and inversion: *Geophysics*, **66**, No. 6, 1856–1863.
- Tarantola, A., 1984, Inversion of seismic reflection data in the acoustic approximation: *Geophysics*, **49**, 1259–1266.

Virieux, A., and Operto, S., 2009, An overview of full-waveform inversion in exploration geophysics: *Geophysics*, **74**, 1259–1266.